

Unsteady flows, turbulent flows

# Interactive boundary layers in turbulent flow

Jean Cousteix<sup>a,b,\*</sup>, Jacques Mauss<sup>c</sup>

<sup>a</sup> Département modèles pour l'aérodynamique et l'énergétique, ONERA, 2 avenue Édouard-Belin, B.P. 4025, 31055 Toulouse cedex 4, France

<sup>b</sup> École nationale supérieure de l'aéronautique et de l'espace, 10, avenue Édouard-Belin, 31055 Toulouse cedex, France

<sup>c</sup> Institut de mécanique des fluides de Toulouse UMR-CNRS et Université Paul-Sabatier, 118, route de Narbonne, 31062 Toulouse cedex, France

Received 16 November 2006; accepted after revision 12 February 2007

Available online 24 September 2007

## Abstract

An asymptotic analysis of the structure of the flow at high Reynolds number around a streamlined body is presented. The boundary layer is turbulent. This question is studied with the successive complementary expansion method, SCEM. The starting point is to look for a uniformly valid approximation (UVA) of the velocity field, including the boundary layer and the external flow. Thanks to the use of generalized expansions, SCEM leads to the theory of interactive boundary layer, IBL. For many years, IBL model has been used successfully to calculate aerodynamic flows. Here, the IBL model is fully justified with rational mathematical arguments. The construction of a UVA of the velocity profile in the boundary layer is also studied. **To cite this article: J. Cousteix, J. Mauss, C. R. Mecanique 335 (2007).**

© 2007 Académie des sciences. Published by Elsevier Masson SAS. All rights reserved.

## Résumé

**Couche limite interactive en écoulement turbulent.** On présente une analyse asymptotique de la structure de l'écoulement à grand nombre de Reynolds en présence d'un corps profilé. La couche limite est turbulente. Avec la méthode des approximations successives complémentaires, MASC, le point de départ est la recherche d'une approximation uniformément valable, AUV, du champ de vitesse couvrant la couche limite et l'écoulement extérieur. Grâce à l'utilisation de développements généralisés, la MASC conduit à la théorie de couche limite interactive, CLI. Les modèles CLI, appliqués depuis longtemps au calcul d'écoulements aérodynamiques, sont ici pleinement justifiés à l'aide d'arguments mathématiques rationnels. La construction d'une AUV pour le profil de vitesse dans la couche limite est également étudiée. **Pour citer cet article : J. Cousteix, J. Mauss, C. R. Mecanique 335 (2007).**

© 2007 Académie des sciences. Published by Elsevier Masson SAS. All rights reserved.

**Keywords:** Turbulence; Interactive boundary layer; Viscous–inviscid flow coupling; Turbulent flow; Asymptotic analysis

**Mots-clés :** Turbulence ; Couche limite interactive ; Couplage visqueux–non visqueux ; Écoulement turbulent ; Analyse asymptotique

## 1. Introduction

The three-dimensional unsteady Navier–Stokes equations apply to turbulent flow if the values of dependent variables are understood as instantaneous values. A direct approach to solving the equations for turbulent flows is to

\* Corresponding author.

E-mail addresses: [Jean.Cousteix@oncert.fr](mailto:Jean.Cousteix@oncert.fr) (J. Cousteix), [mauss@cict.fr](mailto:mauss@cict.fr) (J. Mauss).

solve them for specific boundary conditions and initial values that include time-dependent quantities. Mean values are needed in most practical cases, so an ensemble of solutions of time-dependent equations is required. Even for the most restricted cases, this approach, referred to as direct numerical simulation, becomes a difficult and extremely expensive computing problem because the unsteady eddy motions of turbulence appear over a wide range. The usual procedure is to average the equations rather than their solutions [1]. The averaged Navier–Stokes equations are also called Reynolds equations. The numerical solution of these equations requires the use of a turbulence model as suggested by Boussinesq for the first time [2].

Here, the averaged Navier–Stokes equations are used to study the structure of the flow past a solid wall at high Reynolds number. According to standard results described by the method of matched asymptotic expansions, MMAE, the boundary layer is decomposed into outer and inner regions. The corresponding scales are given in Section 3. With these scales, the application of the successive complementary expansion method, SCEM, Section 2, leads to an interactive boundary layer model, IBL, Sections 4 and 5. In addition, the study of the contribution of the inner region enables us to construct simply an approximation of the velocity profile valid in the whole boundary layer, as far as the velocity profile is known in the outer region, Section 6. Numerical results obtained with a turbulence model à la Boussinesq are presented for a flat plate boundary layer at different Reynolds numbers.

The purpose of this article is not to produce results of calculations using IBL. This work has been done by many authors who proved that the use of IBL is very fruitful [3–6]. Neither is the aim to discuss turbulence models. The purpose here is to justify IBL in turbulent flow using rational arguments based on an asymptotic analysis of the Navier–Stokes equations. Until now, such a justification was lacking.

## 2. Successive complementary expansion method

We consider a singular perturbation problem where the function  $\Phi(y, \varepsilon)$  is defined in a domain  $D$  and  $\varepsilon$  is the small parameter. We assume that two significant subdomains have been identified, an outer and an inner domains. In the outer domain, the relevant variable is  $y$ . We assume that the inner domain is located near the origin and the boundary layer variable is  $Y = y/\zeta(\varepsilon)$  where  $\zeta(\varepsilon)$  is the order of the thickness of the boundary layer. According to the Successive Complementary Expansions Method (SCEM) [7], we represent the function  $\Phi$  by the sum

$$\Phi_a(y, Y, \varepsilon) = \sum_{i=1}^n \bar{\delta}_i(\varepsilon) [\bar{\varphi}_i(y, \varepsilon) + \bar{\psi}_i(Y, \varepsilon)] \tag{1}$$

and we assume that  $\Phi_a$  is a uniformly valid approximation, UVA, of  $\Phi$  defined to order  $\bar{\delta}_n$

$$\Phi = \Phi_a + o(\bar{\delta}_n) \tag{2}$$

The UVA is said *generalized*. It is constructed so that it can be written in the form

$$\Phi_a = \Phi_{ar} + o(\delta_m) \tag{3}$$

where  $\Phi_{ar}$  is a *regular* UVA such that  $\bar{\delta}_n = O(\delta_m)$

$$\Phi_{ar}(y, Y, \varepsilon) = \sum_{i=1}^m \delta_i(\varepsilon) [\varphi_i(y) + \psi_i(Y)] \tag{4}$$

The sequence of order functions  $\bar{\delta}_i$  may or may not be the same as the sequence  $\delta_i$ . In addition, the functions  $\delta_i$  are *gauge functions*, i.e.,  $\delta_i$  is a suitable representative order function chosen in the corresponding equivalence class defined from the relation of strict order  $O_S$ .

The difference between the generalized and regular expansions is that  $\bar{\varphi}_i$  is a function of  $y$  and  $\varepsilon$  whereas  $\varphi_i$  is a function of  $y$  only; in the same way,  $\bar{\psi}_i$  is a function of  $Y$  and  $\varepsilon$  whereas  $\psi_i$  is a function of  $Y$  only.

The idea of producing UVAs to avoid matching is not new and various methods have been devised to achieve this goal; the multi-scaling approach of Mahony [8] is an example. SCEM belongs to a general class of multi-variable expansion methods and the regular version proposed by O’Malley has been used to analyze different perturbation problems [9]. What is new here is that SCEM is used not only to obtain directly a UVA but also to take advantage of the generalized form; this point is crucial.

### 3. Results of the standard asymptotic analysis

The objective of this section is to summarize the main results obtained from the standard asymptotic analysis, i.e. the method of matched asymptotic expansion, MMAE. It is not the purpose of this paper to reestablish these results. The description of the boundary layer is based on experimental observations which can be subject to different interpretations. Here we adopt the point of view described for example by Panton [10] but other authors do not share the same beliefs [11].

#### 3.1. Averaged Navier–Stokes equations

The study of incompressible turbulent flows is addressed by defining a mean flow from a *statistical average* of velocity and of pressure. The instantaneous flow is decomposed into a mean and fluctuating flow

$$\begin{aligned}\tilde{u}_i &= \mathcal{U}_i + \mathcal{U}'_i \\ \tilde{p} &= \mathcal{P} + \mathcal{P}'\end{aligned}$$

An orthonormal axis system is used. The  $x$ -axis is along the wall and the  $y$ -axis is normal to it. All the quantities are dimensionless. The coordinates  $x$  and  $y$  are reduced by the reference length  $L$ , the velocity components by a reference velocity  $V$ , the pressure and the turbulent stresses by  $\rho V^2$ . In fact, the mean flow scales are chosen to define the reference quantities  $V$  and  $L$ . In two-dimensional, incompressible, steady flow (on the average), the *averaged Navier–Stokes equations* or *Reynolds equations* are

$$\frac{\partial \mathcal{U}}{\partial x} + \frac{\partial \mathcal{V}}{\partial y} = 0 \quad (5a)$$

$$\mathcal{U} \frac{\partial \mathcal{U}}{\partial x} + \mathcal{V} \frac{\partial \mathcal{U}}{\partial y} = -\frac{\partial \mathcal{P}}{\partial x} + \frac{\partial}{\partial x} \left( \mathcal{T}_{xx} + \frac{1}{\mathcal{R}} \frac{\partial \mathcal{U}}{\partial x} \right) + \frac{\partial}{\partial y} \left( \mathcal{T}_{xy} + \frac{1}{\mathcal{R}} \frac{\partial \mathcal{U}}{\partial y} \right) \quad (5b)$$

$$\mathcal{U} \frac{\partial \mathcal{V}}{\partial x} + \mathcal{V} \frac{\partial \mathcal{V}}{\partial y} = -\frac{\partial \mathcal{P}}{\partial y} + \frac{\partial}{\partial x} \left( \mathcal{T}_{xy} + \frac{1}{\mathcal{R}} \frac{\partial \mathcal{V}}{\partial x} \right) + \frac{\partial}{\partial y} \left( \mathcal{T}_{yy} + \frac{1}{\mathcal{R}} \frac{\partial \mathcal{V}}{\partial y} \right) \quad (5c)$$

With  $\rho$  denoting the density and  $\mu$  the dynamic viscosity, the Reynolds number  $\mathcal{R}$  is

$$\mathcal{R} = \frac{\rho V L}{\mu}$$

The *turbulent stresses*  $\mathcal{T}_{ij}$  appear when the Navier–Stokes equations are averaged and they are a consequence of the non-linearity of the convection terms. They are defined from the correlations between velocity fluctuations

$$\mathcal{T}_{ij} = -\langle \mathcal{U}'_i \mathcal{U}'_j \rangle$$

#### 3.2. Scales

In a standard manner, as with MMAE, and on the basis of a large amount of experimental data, the flow is decomposed in two regions: the inviscid region and the boundary layer. The former is treated separately and provides us with the necessary data to calculate the boundary layer. The boundary layer is described by a two-layer structure [12,10,13] consisting of: (i) an outer layer characterized by the thickness  $\delta$  and (ii) an inner layer whose thickness is of order  $\nu/u_\tau$  ( $\nu = \mu/\rho$ ) with  $u_\tau$  denoting the *friction velocity* which is defined from the wall shear stress  $\tau_w$

$$u_\tau = \sqrt{\frac{\tau_w}{\rho}}$$

The *turbulence velocity scale*—denoted by  $\mathbf{u}$ —is identical in the outer and inner regions and is of the order of the friction velocity  $u_\tau$ . In the outer region, the turbulence length scale, of the order  $\delta$ , is denoted by  $\ell$  whereas in the inner region, the length scale is  $\nu/\mathbf{u}$ .

In the outer region, we assume that *the time scale of the transport due to turbulence* ( $\ell/\mathbf{u}$ ) *is of the same order as the time scale of mean flow convection*. We can view this hypothesis as the counterpart, for turbulent flow, of the

hypothesis used for a laminar boundary layer that the viscosity time scale is of the same order as the convection time scale. If the reference quantities  $V$  and  $L$  are chosen as velocity and length scales of the mean flow, we deduce

$$\frac{\ell}{L} = \frac{u}{V} \tag{6}$$

The asymptotic analysis introduces the small parameters  $\varepsilon$  and  $\hat{\varepsilon}$  which define, with dimensionless variables, the order of the thicknesses of the outer and inner layers

$$\varepsilon = \frac{\ell}{L} \tag{7}$$

$$\hat{\varepsilon} = \frac{\nu}{uL} \tag{8}$$

Using (6), we have

$$\varepsilon \hat{\varepsilon} \mathcal{R} = 1 \tag{9}$$

With the skin-friction law (47c), it is shown that the following relation holds

$$\varepsilon = \text{Os}\left(\frac{1}{\ln \mathcal{R}}\right) \tag{10}$$

In particular, we deduce that, for any positive  $n$

$$\varepsilon^n > \hat{\varepsilon} > \frac{1}{\mathcal{R}}$$

The wall being defined by  $y = 0$ , the variables appropriate to the study of each region are

$$\text{Outer region: } \eta = \frac{y}{\varepsilon} \tag{11a}$$

$$\text{Inner region: } \hat{y} = \frac{y}{\hat{\varepsilon}} \tag{11b}$$

#### 4. Application of SCEM

The method employed to construct a UVA comprises three steps: (i) we seek a first approximation corresponding to the external region of the flow; (ii) this approximation is corrected in the outer region of the boundary layer; and finally (iii) a UVA is obtained by taking into account the contribution of the inner region of the boundary layer [7].

##### 4.1. First approximation

We seek a first approximation in the form

$$\mathcal{U} = u_1^*(x, y, \varepsilon) + \dots \tag{12a}$$

$$\mathcal{V} = v_1^*(x, y, \varepsilon) + \dots \tag{12b}$$

$$\mathcal{P} = p_1^*(x, y, \varepsilon) + \dots \tag{12c}$$

$$\mathcal{T}_{ij} = 0 \tag{12d}$$

Putting these expansions in (5a)–(5c) and neglecting  $O(1/\mathcal{R})$  terms, it can be shown that  $u_1^*, v_1^*, p_1^*$  satisfy the Euler equations. It is required to complement the above approximation because the no-slip condition at the wall cannot be satisfied. Moreover, the wall condition for  $v_1^*$  is not known, see Section 5.3.4.

##### 4.2. Contribution of the outer region of the boundary layer

A correction to the previous approximation is introduced in the form of a contribution of the outer region of the boundary layer

$$\mathcal{U} = u_1^*(x, y, \varepsilon) + \varepsilon U_1(x, \eta, \varepsilon) + \dots \quad (13a)$$

$$\mathcal{V} = v_1^*(x, y, \varepsilon) + \varepsilon^2 V_1(x, \eta, \varepsilon) + \dots \quad (13b)$$

$$\mathcal{P} = p_1^*(x, y, \varepsilon) + \Delta(\varepsilon) P_1(x, \eta, \varepsilon) + \dots \quad (13c)$$

$$\mathcal{T}_{ij} = \varepsilon^2 \tau_{ij,1}(x, \eta, \varepsilon) + \dots \quad (13d)$$

The gauges for the velocity and for the Reynolds stresses are chosen according to the standard asymptotic analysis. The gauge  $\Delta(\varepsilon)$  is determined by examining the  $y$ -momentum equation.

#### 4.2.1. Gauge for the pressure

Taking into account the Euler equations, the  $y$ -momentum equation can be written as

$$\begin{aligned} \varepsilon U_1 \frac{\partial v_1^*}{\partial x} + \varepsilon^2 u_1^* \frac{\partial V_1}{\partial x} + \varepsilon^3 U_1 \frac{\partial V_1}{\partial x} + \varepsilon^2 V_1 \frac{\partial v_1^*}{\partial y} + \varepsilon v_1^* \frac{\partial V_1}{\partial \eta} + \varepsilon^3 V_1 \frac{\partial V_1}{\partial \eta} \\ = -\frac{\Delta}{\varepsilon} \frac{\partial P_1}{\partial \eta} + \varepsilon^2 \frac{\partial \tau_{xy,1}}{\partial x} + \frac{1}{\mathcal{R}} \frac{\partial^2 v_1^*}{\partial x^2} + \frac{\varepsilon^2}{\mathcal{R}} \frac{\partial^2 V_1}{\partial x^2} + \varepsilon \frac{\partial \tau_{yy,1}}{\partial \eta} + \frac{1}{\mathcal{R}} \frac{\partial^2 v_1^*}{\partial y^2} + \frac{1}{\mathcal{R}} \frac{\partial^2 V_1}{\partial \eta^2} \end{aligned}$$

In the boundary layer, by using the continuity equation, the Taylor series expansion of  $v_1^*$  when  $y \ll 1$  yields

$$v_1^* = v_{1y=0}^* + y \left( \frac{\partial v_1^*}{\partial y} \right)_{y=0} + \dots = v_{1y=0}^* - y \left( \frac{\partial u_1^*}{\partial x} \right)_{y=0} + \dots = v_{1y=0}^* - \varepsilon \eta \left( \frac{\partial u_1^*}{\partial x} \right)_{y=0} + \dots \quad (14)$$

The condition of zero velocity at the wall implies that  $v_{1y=0}^*$  is  $O(\varepsilon^2)$  in order to balance the term  $\varepsilon^2 V_1$  in the expansion (20b) of  $v$  because the next term  $\varepsilon \hat{v}_1$  is smaller. From the last equality in (14), it follows that, in the outer region of the boundary layer,  $v_1^*$  is  $O(\varepsilon)$ . Then, the dominant term of the  $y$ -momentum equation is  $\varepsilon \frac{\partial \tau_{yy,1}}{\partial \eta}$  which must be balanced by the pressure term. It is concluded that  $\Delta$  is  $O(\varepsilon^2)$ . We set

$$\Delta = \varepsilon^2 \quad (15)$$

Then, the  $y$ -momentum equation becomes

$$-\frac{\partial P_1}{\partial \eta} + \frac{\partial \tau_{yy,1}}{\partial \eta} = O(\varepsilon)$$

According to the SCEM principle, as  $\eta \rightarrow \infty$ , we must have  $P_1 \rightarrow 0$  and  $\tau_{yy,1} \rightarrow 0$ . Then, neglecting terms of order  $O(\varepsilon)$ , we have

$$-P_1 + \tau_{yy,1} = 0 \quad (16)$$

#### 4.2.2. Continuity equation

Taking into account the continuity equation relating  $u_1^*$  and  $v_1^*$ , we have

$$\frac{\partial U_1}{\partial x} + \frac{\partial V_1}{\partial \eta} = 0 \quad (17)$$

#### 4.2.3. $x$ -Momentum equation

Expansions (13a)–(13d) are substituted in (5b) and the Euler equations for  $u_1^*$ ,  $v_1^*$ ,  $p_1^*$  are taken into account. Then, if  $O(\varepsilon^2)$  terms are neglected, the  $x$ -momentum equation (5b) becomes

$$U_1 \frac{\partial u_1^*}{\partial x} + u_1^* \frac{\partial U_1}{\partial x} + \frac{v_1^*}{\varepsilon} \frac{\partial U_1}{\partial \eta} = \frac{\partial \tau_{xy,1}}{\partial \eta} \quad (18)$$

If  $O(\varepsilon^3)$  terms are neglected, the  $x$ -momentum equation (5b) becomes

$$U_1 \frac{\partial u_1^*}{\partial x} + u_1^* \frac{\partial U_1}{\partial x} + \varepsilon U_1 \frac{\partial U_1}{\partial x} + \varepsilon V_1 \frac{\partial u_1^*}{\partial y} + \frac{v_1^*}{\varepsilon} \frac{\partial U_1}{\partial \eta} + \varepsilon V_1 \frac{\partial U_1}{\partial \eta} = \frac{\partial \tau_{xy,1}}{\partial \eta} + \varepsilon \left( \frac{\partial \tau_{xx,1}}{\partial x} - \frac{\partial \tau_{yy,1}}{\partial x} \right) \quad (19)$$

For both models, described by (18) or (19), the boundary conditions as  $\eta \rightarrow \infty$  are

$$\eta \rightarrow \infty: \quad U_1 \rightarrow 0, \quad V_1 \rightarrow 0$$

With these conditions and by taking into account the vanishing of the turbulent stresses in the inviscid flow, we observe that (18) or (19) are perfectly satisfied as  $\eta \rightarrow \infty$ . The wall boundary conditions are given later in Section 5. Before, we have to study the contribution of the inner region.

*4.3. Contribution of the inner region of the boundary layer*

We seek a UVA in the form

$$U = u_1^*(x, y, \varepsilon) + \varepsilon U_1(x, \eta, \varepsilon) + \varepsilon \widehat{U}_1(x, \hat{y}, \varepsilon) + \dots \tag{20a}$$

$$V = v_1^*(x, y, \varepsilon) + \varepsilon^2 V_1(x, \eta, \varepsilon) + \varepsilon \hat{\varepsilon} \widehat{V}_1(x, \hat{y}, \varepsilon) + \dots \tag{20b}$$

$$P = p_1^*(x, y, \varepsilon) + \varepsilon^2 P_1(x, \eta, \varepsilon) + \widehat{\Delta}(\varepsilon) \widehat{P}_1(x, \hat{y}, \varepsilon) + \dots \tag{20c}$$

$$T_{ij} = \varepsilon^2 \tau_{ij,1}(x, \eta, \varepsilon) + \varepsilon^2 \hat{\tau}_{ij,1}(x, \hat{y}, \varepsilon) + \dots \tag{20d}$$

The gauge  $\widehat{\Delta}$  is determined by examining the  $y$ -momentum equation.

*4.3.1. Gauge for the pressure*

Expansions (20a)–(20d) are substituted in (5c) and, from inspection of the resulting equation, we are led to choose

$$\widehat{\Delta} = \varepsilon^2 \tag{21}$$

and the  $y$ -momentum equation becomes

$$-\frac{\partial \widehat{P}_1}{\partial \hat{y}} + \frac{\partial \hat{\tau}_{yy,1}}{\partial \hat{y}} = 0 \tag{22}$$

*4.3.2. Continuity equation*

For the velocity components  $\widehat{U}_1$  and  $\widehat{V}_1$ , we have

$$\frac{\partial \widehat{U}_1}{\partial x} + \frac{\partial \widehat{V}_1}{\partial \hat{y}} = 0 \tag{23}$$

*4.3.3. x-Momentum equation*

Expansions (20a)–(20d) are substituted in (5b) and the Euler equations for  $u_1^*, v_1^*, p_1^*$  are taken into account. Then, analyzing the order of various terms, taking into account (18) and retaining only  $O(\varepsilon^2/\hat{\varepsilon})$  terms, the  $x$ -momentum equation (5b) reduces to

$$\frac{\varepsilon^2}{\hat{\varepsilon}} \frac{\partial \hat{\tau}_{xy,1}}{\partial \hat{y}} + \frac{1}{\varepsilon \mathcal{R}} \frac{\partial^2 U_1}{\partial \eta^2} + \frac{\varepsilon}{\hat{\varepsilon}^2 \mathcal{R}} \frac{\partial^2 \widehat{U}_1}{\partial \hat{y}^2} = 0 \tag{24}$$

A better approximation consistent with the second approximation of the contribution of the outer region of the boundary layer is obtained by retaining  $O(\varepsilon^3/\hat{\varepsilon})$  terms in the  $x$ -momentum equation. Taking into account (19), (5b) becomes

$$\frac{\varepsilon}{\hat{\varepsilon}} v_1^* \frac{\partial \widehat{U}_1}{\partial \hat{y}} + \frac{\varepsilon^3}{\hat{\varepsilon}} V_1 \frac{\partial \widehat{U}_1}{\partial \hat{y}} = \frac{\varepsilon^2}{\hat{\varepsilon}} \frac{\partial \hat{\tau}_{xy,1}}{\partial \hat{y}} + \frac{1}{\varepsilon \mathcal{R}} \frac{\partial^2 U_1}{\partial \eta^2} + \frac{\varepsilon}{\hat{\varepsilon}^2 \mathcal{R}} \frac{\partial^2 \widehat{U}_1}{\partial \hat{y}^2} \tag{25}$$

**5. Interactive boundary layer**

The UVA is obtained from (20a)–(20d). According to the order of neglected terms in the  $x$ -momentum equation, we obtain a first or second order IBL model. In order to have a more compact system of equations, it is possible to include the contributions of the outer and inner regions of the boundary layer in a single set of equations which is called below ‘global model’. Finally, in this section, we present simplifications of the model when the external flow is irrotational.

### 5.1. First and second order models

The *first order IBL* model comprises (17), (18), (23) and (24). In addition,  $u_1^*$  and  $v_1^*$  satisfy the Euler equations. The boundary conditions are

$$\eta \rightarrow \infty: U_1 \rightarrow 0, \quad V_1 \rightarrow 0 \quad (26a)$$

$$\hat{y} \rightarrow \infty: \hat{U}_1 \rightarrow 0, \quad \hat{V}_1 \rightarrow 0 \quad (26b)$$

and, at the wall

$$u_1^* + \varepsilon U_1 + \varepsilon \hat{U}_1 = 0 \quad (27a)$$

$$v_1^* + \varepsilon^2 V_1 + \hat{\varepsilon} \hat{V}_1 = 0 \quad (27b)$$

At infinity, we also have conditions on  $u_1^*$  and  $v_1^*$ , usually corresponding to uniform flow conditions.

The *second order IBL* model comprises (17), (19), (23) and (25). This system must be associated with Euler equations for  $u_1^*$  and  $v_1^*$ . The boundary conditions are identical to those of the first order model.

### 5.2. Global model

The models presented above can be included in a global model having the following properties: (i) the global model describes the outer and the inner boundary layer regions (ii) the global model contains the first and the second order IBL models.

We set

$$u = u_1^* + \varepsilon U_1 + \varepsilon \hat{U}_1 \quad (28a)$$

$$v = v_1^* + \varepsilon^2 V_1 + \varepsilon \hat{\varepsilon} \hat{V}_1 \quad (28b)$$

$$-\langle u'_i u'_j \rangle = \varepsilon^2 \tau_{ij,1} + \varepsilon^2 \hat{\tau}_{ij,1} \quad (28c)$$

The equations proposed below for  $u$  and  $v$  cannot be deduced from any model established before. This is a heuristic model which can be written as

$$\frac{\partial u}{\partial x} + \frac{\partial v}{\partial y} = 0 \quad (29a)$$

$$u \frac{\partial u}{\partial x} + v \frac{\partial u}{\partial y} = u_1^* \frac{\partial u_1^*}{\partial x} + v_1^* \frac{\partial u_1^*}{\partial y} + \frac{\partial}{\partial y} (-\langle u'v' \rangle) + \frac{1}{\mathcal{R}} \frac{\partial^2 (u - u_1^*)}{\partial y^2} + \frac{\partial}{\partial x} (\langle v'^2 \rangle - \langle u'^2 \rangle) \quad (29b)$$

It can be checked that the equations of second order IBL (17), (19), (23) and (25) are recovered after expanding (29a), (29b) according to the method discussed in Section 4. Eqs. (29a), (29b) must be associated with the Euler equations for  $u_1^*$  and  $v_1^*$ . Using (26a), (26b), (27a), (27b) and (28a), (28b), we obtain the boundary conditions

$$y \rightarrow \infty: u - u_1^* \rightarrow 0, \quad v - v_1^* \rightarrow 0 \quad (30a)$$

$$\text{at the wall: } u = 0, \quad v = 0 \quad (30b)$$

As discussed in Section 5.3.4, condition (30a) on  $v$  implies an interaction between the boundary layer and the inviscid flow because the wall value of  $v_1^*$  required to satisfy (30a) depends on the boundary layer results so that the inviscid flow equations can not be solved independently from the boundary layer equations.

### 5.3. Reduced model for an irrotational external flow

For an *external irrotational flow*, the global model of Section 5.2 takes a simplified form if the validity of equations is restricted to the boundary layer region.

**5.3.1. Outer region of the boundary layer**

As the boundary layer thickness is small compared to 1, we have  $y \ll 1$  in the boundary layer, and Taylor series expansions can be used to express the characteristics of the external flow in the boundary layer, for example

$$u_1^* = u_{1y=0}^* + y \left( \frac{\partial u_1^*}{\partial y} \right)_{y=0} + \dots = u_{1y=0}^* + \varepsilon \eta \left( \frac{\partial u_1^*}{\partial y} \right)_{y=0} + \dots$$

In addition, we assume that the inviscid flow is irrotational and that the wall curvature effects are negligible. Then, approximations (13a)–(13d) give [7]

$$\begin{aligned} \mathcal{U} &= u_{10}^* + \varepsilon U_1 + \dots \\ \mathcal{V} &= v_{10}^* - y u_{1x0}^* + \varepsilon^2 V_1 + \dots \\ \mathcal{T}_{ij} &= \varepsilon^2 \tau_{ij,1} + \dots \end{aligned}$$

where index “0” means a value at the wall and index  $x$  means an  $x$ -derivative. With the hypotheses stated above, (17) and (19) restricted to the outer region of the boundary layer become

$$\frac{\partial U_1}{\partial x} + \frac{\partial V_1}{\partial \eta} = 0 \tag{31a}$$

$$U_1 \frac{du_{10}^*}{dx} + u_{10}^* \frac{\partial U_1}{\partial x} + \varepsilon U_1 \frac{\partial U_1}{\partial x} + \frac{v_{10}^* - y u_{1x0}^*}{\varepsilon} \frac{\partial U_1}{\partial \eta} + \varepsilon V_1 \frac{\partial U_1}{\partial \eta} = \frac{\partial \tau_{xy,1}}{\partial \eta} + \varepsilon \left( \frac{\partial \tau_{xx,1}}{\partial x} - \frac{\partial \tau_{yy,1}}{\partial x} \right) \tag{31b}$$

**5.3.2. Inner region of the boundary layer**

In the same way as in the outer region, the equations for the contribution of the inner region can be simplified. Expansions (20a)–(20d), written in the boundary layer, give

$$\begin{aligned} \mathcal{U} &= u_{10}^* + \varepsilon U_1 + \varepsilon \widehat{U}_1 + \dots \\ \mathcal{V} &= v_{10}^* - y u_{1x0}^* + \varepsilon^2 V_1 + \varepsilon \widehat{\varepsilon} \widehat{V}_1 + \dots \\ \mathcal{T}_{ij} &= \varepsilon^2 \tau_{ij,1} + \varepsilon^2 \widehat{\tau}_{ij,1} + \dots \end{aligned}$$

Eqs. (23) and (25), restricted to the inner region of the boundary layer, become

$$\frac{\partial \widehat{U}_1}{\partial x} + \frac{\partial \widehat{V}_1}{\partial \widehat{y}} = 0 \tag{32a}$$

$$\frac{\varepsilon}{\widehat{\varepsilon}} v_{10}^* \frac{\partial \widehat{U}_1}{\partial \widehat{y}} + \frac{\varepsilon^3}{\widehat{\varepsilon}} V_1 \frac{\partial \widehat{U}_1}{\partial \widehat{y}} = \frac{\varepsilon^2}{\widehat{\varepsilon}} \frac{\partial \widehat{\tau}_{xy,1}}{\partial \widehat{y}} + \frac{1}{\varepsilon \mathcal{R}} \frac{\partial^2 U_1}{\partial \eta^2} + \frac{\varepsilon}{\widehat{\varepsilon}^2 \mathcal{R}} \frac{\partial^2 \widehat{U}_1}{\partial \widehat{y}^2} \tag{32b}$$

**5.3.3. Global reduced model**

We set

$$u = u_{10}^* + \varepsilon U_1 + \varepsilon \widehat{U}_1 \tag{33a}$$

$$v = v_{10}^* - y u_{1x0}^* + \varepsilon^2 V_1 + \varepsilon \widehat{\varepsilon} \widehat{V}_1 \tag{33b}$$

$$t_{ij} = -\langle u'_i u'_j \rangle = \varepsilon^2 \tau_{ij,1} + \varepsilon^2 \widehat{\tau}_{ij,1} \tag{33c}$$

Eqs. (31a), (31b) and (32a), (32b) are contained in the following heuristic model, valid only in the boundary layer

$$\frac{\partial u}{\partial x} + \frac{\partial v}{\partial y} = 0 \tag{34a}$$

$$u \frac{\partial u}{\partial x} + v \frac{\partial u}{\partial y} = u_{10}^* \frac{du_{10}^*}{dx} + \frac{\partial}{\partial y} (-\langle u'v' \rangle) + \frac{1}{\mathcal{R}} \frac{\partial^2 u}{\partial y^2} + \frac{\partial}{\partial x} (\langle v'^2 \rangle - \langle u'^2 \rangle) \tag{34b}$$

with the boundary conditions

$$y \rightarrow \infty: \quad u - u_{10}^* \rightarrow 0, \quad v - v_{10}^* + y u_{1x0}^* \rightarrow 0 \tag{35a}$$

$$\text{at the wall:} \quad u = 0, \quad v = 0 \tag{35b}$$

**Remark.** The boundary condition (35a) on  $v$  can be interpreted in terms of displacement thickness  $\delta_1$ . Using the continuity equation, it is easy to show that

$$v_{10}^* = \frac{d(u_{10}^* \delta_1)}{dx} \quad \text{with } \delta_1 = \int_0^\infty \left(1 - \frac{u}{u_{10}^*}\right) dy$$

Very often, the contribution of term  $\frac{\partial}{\partial x}(\langle v'^2 \rangle - \langle u'^2 \rangle)$  in (34b) is neglected because experimental results show that the values of  $\langle u'^2 \rangle$  and  $\langle v'^2 \rangle$  are close; in a first order model, this term is not present. With this hypothesis, we obtain the standard boundary layer equations which are generally used

$$\frac{\partial u}{\partial x} + \frac{\partial v}{\partial y} = 0 \quad (36a)$$

$$u \frac{\partial u}{\partial x} + v \frac{\partial u}{\partial y} = u_{10}^* \frac{du_{10}^*}{dx} + \frac{\partial}{\partial y}(-\langle u'v' \rangle) + \frac{1}{\mathcal{R}} \frac{\partial^2 u}{\partial y^2} \quad (36b)$$

#### 5.3.4. Discussion

The interactive character of the models presented in Section 5.1 or Section 5.2 or Section 5.3.3 comes from condition (30a) or (35a) on  $v$ . This condition requires that the inviscid flow equations and the boundary layer equations must be solved simultaneously. It is not possible to solve the Euler equations independently from the boundary layer equations because the wall condition on  $v_1^*$  depends on the boundary layer results. In practice, the value of  $v_1^*$  at the wall can be determined iteratively in order to satisfy condition (30a) or (35a) on  $v$ . The two systems of equations interact; one system influences the other system and vice versa. One of the most important strength of IBL methods is that separated flows can be calculated if appropriate numerical techniques are implemented [3–6].

The IBL model is obtained thanks to the use of *generalized expansions*. If SCEM is applied with *regular expansions*, it can be shown that MMAE results are obtained. In particular, the second boundary condition at infinity (35a) reduces to  $v_{10}^* = 0$ . With this condition, the Euler equations can be solved *independently* from the boundary layer equations and the interactive character disappears. The boundary layer equations are solved with a prescribed distribution of  $u_{10}^*$  obtained from the solution of Euler equations and the following boundary conditions are applied to the boundary layer equations

$$y \rightarrow \infty: \quad u - u_{10}^* \rightarrow 0 \quad (37a)$$

$$\text{at the wall: } \quad u = 0, \quad v = 0 \quad (37b)$$

This model corresponds to Prandtl's formulation.

## 6. Approximation of the boundary layer velocity profile

### 6.1. Formulation of the problem

The objective is to construct an approximation of the velocity profile *in the whole boundary layer* for an external irrotational flow. For this, we use (24) which describes the first order contribution of the boundary layer inner region. The solution for  $\widehat{U}_1$  requires the knowledge of the function  $U_1(\eta)$  and the implementation of a turbulence model to describe the evolution of  $\widehat{\tau}_{xy,1}$ . The study relies on a mixing length scheme, particularly well adapted to a flat plate flow, and on similarity solutions for the outer region of the boundary layer [14].

Rather than solve (24), it is more convenient to use an equation which gives directly the total velocity. We return to expansion given by (33c) and write (24) in the form

$$\frac{\varepsilon^2}{\widehat{\varepsilon}} \frac{\partial}{\partial \widehat{y}} \left( \frac{t_{xy}}{\varepsilon^2} - \tau_{xy,1} \right) + \frac{1}{\varepsilon \mathcal{R}} \frac{\partial^2 U_1}{\partial \eta^2} + \frac{\varepsilon}{\widehat{\varepsilon}^2 \mathcal{R}} \frac{\partial^2 \widehat{U}_1}{\partial \widehat{y}^2} = 0 \quad (38)$$

Now, for an external irrotational flow, (33a) holds and  $u_{10}^*$  does not depend on  $y$ , so that (38) can be written as

$$\frac{\partial}{\partial y} \left[ t_{xy} + \frac{1}{\mathcal{R}} \frac{\partial u}{\partial y} \right] = \varepsilon^2 \frac{\partial \tau_{xy,1}}{\partial y} \quad (39)$$

The left-hand side of (39) represents the total stress—sum of the turbulent and viscous stresses—in the whole boundary layer whereas the right-hand side represents the turbulent stress in the outer region. Let us integrate this equation with respect to  $y$  from the wall  $y = 0$ . The dimensionalized wall shear stress being  $\tau_w$ , we obtain

$$t_{xy} + \frac{1}{\mathcal{R}} \frac{\partial u}{\partial y} - \frac{\tau_w}{\varrho V^2} = \varepsilon^2 \tau_{xy,1} - \frac{\tau_w}{\varrho V^2} \tag{40}$$

because, at  $y = 0$ , we have

$$\frac{\tau_w}{\varrho V^2} = \frac{1}{\mathcal{R}} \frac{\partial u}{\partial y} \quad \text{and} \quad t_{xy} = 0$$

and, on the other hand, the outer solution is such that we have as  $\eta \rightarrow 0$ , i.e. at  $y = 0$

$$\varepsilon^2 \tau_{xy,1} = \frac{\tau_w}{\varrho V^2}$$

Finally, (40) takes the form

$$t_{xy} + \frac{1}{\mathcal{R}} \frac{\partial u}{\partial y} = \varepsilon^2 \tau_{xy,1}$$

Synthetically, by dividing the two members by the dimensionless wall shear stress, the above equation becomes

$$\frac{\tau}{\tau_w} = \frac{\tau_{out}}{\tau_w} \tag{41}$$

where the left-hand side represents the dimensionless total stress in the whole boundary layer and the right-hand side represents the approximation of the dimensionless turbulent stress calculated in the outer region of the boundary layer. The solution of (41) gives a UVA of the velocity profile in the whole boundary layer and not only an approximation in the inner region. We can note that (41) enables us to satisfy the boundary conditions on the total stress. Indeed, at  $y = 0$  we have  $\tau/\tau_w = 1$  and at  $y = \delta$  we have  $\tau/\tau_w = 0$ . This result is due to the behaviour of the solution in the outer region (right-hand side of (41)).

**Remark.** Following the standard asymptotic theory (MMAE), the right-hand side of (41) is equal to 1 if the solution is sought in the inner region. Indeed,  $\tau_{out}/\tau_w$  is a function of  $\eta$ . Now, we have  $\eta = \hat{y}\hat{\varepsilon}/\varepsilon$  and, for the study of the inner region,  $\hat{y}$  is kept fixed and  $\hat{\varepsilon}/\varepsilon \rightarrow 0$ . Therefore, the value of the right-hand side of (41) must be taken at  $\eta = 0$ . This value is 1 and we find exactly the inner region equation obtained with MMAE,  $\tau/\tau_w = 1$ .

### 6.2. Turbulence model

Coming back to dimensionalized variables, including the distance to the wall  $y$ , the total stress  $\tau$  in the left-hand side of (41) is

$$\tau = -\varrho \langle u'v' \rangle + \mu \frac{\partial u}{\partial y} \tag{42}$$

A turbulence model is required to express the turbulent stress  $-\varrho \langle u'v' \rangle$ . The turbulence modelling problem has been approached by Boussinesq for the first time and since then, this topic is still under development. In many fields, a good turbulence model is the key for the good prediction of the flow. Very refined turbulence models exist today [1] but there is no universal model able to predict any type of turbulent flow. Very often, a specific model can be used with confidence if its application is restricted to a certain class of flows. Here, for the purpose of demonstration, we are interested in flat plate flows. To this end, a mixing length scheme is well adapted. It must be stressed, however, that the conclusions which can be drawn depend on the validity of the turbulence model. Such a discussion is out of the scope of this article. This work has been done elsewhere [14] with the use of comparisons with experimental data. Here, the purpose is to show that SCEM leads to consistent results, in particular in comparison with the standard approach.

The mixing length model, which can be put in a Boussinesq form, has been proposed by Prandtl and has been refined later [4,14]. The model used here is given by [14]

$$-\varrho \langle u'v' \rangle = \varrho F_c^2 \ell^2 \left( \frac{\partial u}{\partial y} \right)^2 \tag{43a}$$

$$\frac{\ell}{\delta} = 0.085 \text{th} \frac{\chi}{0.085} \frac{y}{\delta}, \quad \chi = 0.41 \tag{43b}$$

$$F_c = 1 - \exp \left[ -(\tau \varrho)^{1/2} \frac{\ell}{26\chi\mu} \right] \tag{43c}$$

In the inner region, by setting  $\tau = \tau_w$  and  $\ell = \chi y$ , the *damping function*  $F_c$  takes the form proposed by Van Driest [15] which can be expressed with the wall variable  $y^+ = yu_\tau/\nu$

$$F_c = 1 - \exp \left( -\frac{y^+}{26} \right)$$

### 6.3. Outer region

In order to solve (41), we need to know  $\tau_{\text{out}}/\tau_w$ , i.e. the solution of the outer region. According to experimental results, in particular for a flat plate flow, the outer region of the boundary layer is well described by *similarity solutions* [16–20]. We assume that the *velocity defect* is a function of  $y/\delta$  where  $\delta$  is the boundary layer thickness

$$\frac{u_e - u}{u_\tau} = F'(\eta) \quad \text{with } \eta = \frac{y}{\delta} \text{ and } u_\tau = \sqrt{\frac{\tau_w}{\varrho}}$$

Usually, the quantity  $(u_e - u)/u_\tau$  is called velocity defect because it represents a defect of the velocity with respect to the external velocity  $u_e$ . The similarity equation of the outer region is [14]

$$\frac{\tau_{\text{out}}}{\tau_w} = 1 - \frac{F}{F_1} + \left( \frac{1}{F_1} + 2\beta \right) \eta F' \tag{44}$$

where

$$F = \int_0^\eta F' d\eta, \quad F_1 = F(1), \quad \beta = -\frac{\delta}{u_\tau} \frac{du_e}{dx}$$

In the outer region of the boundary layer, the stress  $\tau_{\text{out}}$  consists of only the turbulent stress since the viscous stress is negligible. On the other hand, the damping function is equal to 1 because  $y^+ \gg 1$ . Therefore, we have

$$\frac{\tau_{\text{out}}}{\tau_w} = \left( \frac{\ell}{\delta} \right)^2 F''^2 \quad \text{with } F'' = \frac{dF'}{d\eta}$$

For any admissible value of the pressure gradient parameter  $\beta$ , the numerical solution of the similarity equation provides us with a velocity profile  $F'(\eta)$  and the associated turbulent stress profile, i.e. with the notations of Section 6.1 the quantity  $\tau_{\text{out}}/\tau_w$ .

### 6.4. Equation to solve

Given the Reynolds number, the velocity profile in the whole boundary layer is a solution of (41) where the expression of  $\tau$  in the left-hand side is given by (42) and the turbulent stress is expressed by (43a)–(43c).

In (41), the right-hand side is given by the solution of (44) which is the solution of the outer region. Moreover, the Reynolds number or the Kàrmàn number must be fixed. The simplest is to give the value of the Kàrmàn number  $\frac{u_\tau \delta}{\nu}$  which relates directly  $y^+$  and  $\eta$

$$y^+ = \eta \frac{u_\tau \delta}{\nu}$$

With its right-hand side given by the solution of (44), the equation to solve (41), written in wall variables, is a first order ordinary differential equation for  $u^+(y^+)$

$$\frac{\partial u^+}{\partial y^+} + F_c^2 \ell^{+2} \left( \frac{\partial u^+}{\partial y^+} \right)^2 = \frac{\tau_{\text{out}}}{\tau_w} \tag{45}$$

with

$$\ell^+ = \frac{\ell u_\tau}{\nu} = \frac{\ell}{\delta} \frac{u_\tau \delta}{\nu}, \quad u^+ = \frac{u}{u_\tau}, \quad y^+ = \frac{y u_\tau}{\nu}$$

The wall condition is  $u = 0$ , i.e.  $u^+ = 0$  at  $y^+ = 0$ . At the boundary layer edge, the condition  $\tau_{out}/\tau_w = 0$  imposes  $\frac{\partial u}{\partial y} = 0$ ; therefore, we have  $\frac{\partial u^+}{\partial y^+} = 0$  at  $y^+ = \frac{u_\tau \delta}{\nu}$  ( $\eta = 1$ ). At the boundary layer edge, no boundary condition is required to solve (45) but the solution yields a certain value of  $u^+$  which gives the skin-friction coefficient since we have

$$u^+_{y=\delta} = \frac{u_e}{u_\tau} = \frac{1}{\sqrt{Cf/2}} \quad \text{with} \quad \frac{Cf}{2} = \frac{\tau_w}{\rho u_e^2} \tag{46}$$

### 6.5. Examples of results

The results presented in this section have been obtained for a flat plate flow ( $\beta = 0$ ) for different values of the Kàrmàn number. Fig. 1 show a seemingly correct evolution of the velocity *in the whole boundary layer*. We observe that the logarithmic law is present when the Kàrmàn number is large enough. The extent of the logarithmic region measured in wall variables increases when the Kàrmàn number increases. When the Kàrmàn number is too small, the logarithmic region disappears.

The velocity profiles in the region close to the wall are not very much sensitive to the Kàrmàn number. For values of  $u_\tau \delta / \nu > 300$ , the function  $u^+(y^+)$  is practically independent of the Kàrmàn number for  $y^+ < 50$ . In this sense, the velocity law in the inner region is said *universal*. This behaviour is in agreement with the difference in the orders of magnitude between the turbulence length scales (or between the turbulent time scales) in the inner region and in the outer region of the boundary layer. The inner region has a time scale *much smaller* than the outer region. Under these conditions, the inner region acquires its own organization, independently of the parameters which govern the flow in the outer region.

Another way to present the results is to plot the velocity profiles with the outer variables. In Fig. 2, the velocity defect  $(u - u_e)/u_\tau$  is plotted as a function of  $y/\delta$  in semi-logarithmic coordinates. With these variables, for values of  $u_\tau \delta / \nu > 300$ , the outer part of the velocity profile is practically independent of the Kàrmàn number for  $y/\delta > 0.15$ . This observation is valid because we consider only zero pressure gradient boundary layers. In the outer part of the boundary layer, the shape of the velocity defect depends on the pressure gradient. Below  $y/\delta = 0.15$ , for values of the Kàrmàn number larger than 300, a part of the velocity defect profiles exhibits a logarithmic behaviour.

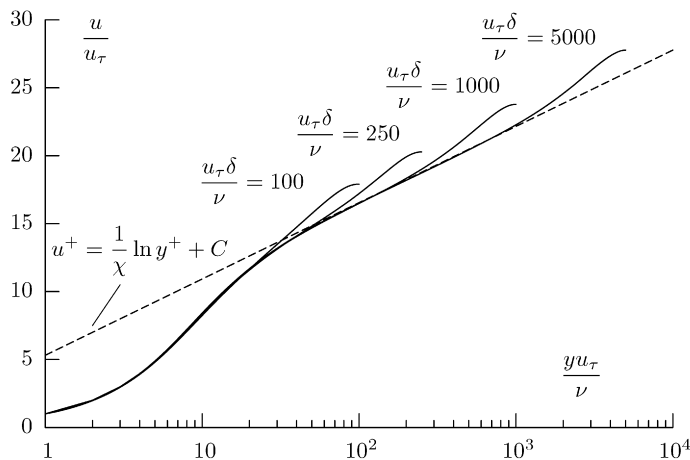


Fig. 1. Approximation of the velocity profiles in a flat plate turbulent boundary layer at different Kàrmàn numbers with inner variables.

Fig. 1. Approximation des profils de vitesses dans une couche limite turbulente de plaque plane à différents nombres de Kàrmàn en variables internes.

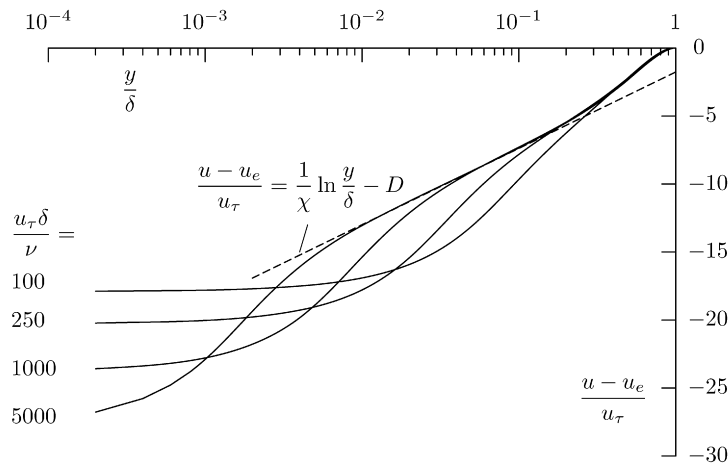


Fig. 2. Approximation of the velocity profiles in a flat plate turbulent boundary layer at different Kármán numbers with outer variables.

Fig. 2. Approximation des profils de vitesses dans une couche limite turbulente de plaque plane à différents nombres de Kármán en variables externes.

It must be stressed again that the values of  $y^+$ ,  $y/\delta$  and of the Kármán number for which the logarithmic behaviour of the velocity is observed depend on the turbulence model which is used. Here, the purpose is not to discuss these points but simply to illustrate the application of SCEM.

The value of the skin-friction coefficient obtained from the value of  $u^+$  at the edge of the boundary layer, see (46), can be compared to the value obtained from the overlap between the law of the wall and the velocity defect law. According to the standard asymptotic analysis, the velocity profile in the inner region of the boundary layer has the form  $u^+ = f(y^+)$  and, in the outer region, the velocity profile has the form  $(u - u_e)/u_\tau = g(\eta)$ . There is an overlap region valid when  $y^+ \gg 1$  and  $\eta \ll 1$  where the velocity profile is logarithmic. More precisely, in the overlap region, we have simultaneously, see Section 6.6

$$\frac{u}{u_\tau} = \frac{1}{\chi} \ln \frac{yu_\tau}{\nu} + C \tag{47a}$$

$$\frac{u_e - u}{u_\tau} = -\frac{1}{\chi} \ln \frac{y}{\delta} + D \tag{47b}$$

The equality of velocities given by the two laws in the overlap region yields

$$\frac{u_e}{u_\tau} = \frac{1}{\chi} \ln \frac{u_\tau \delta}{\nu} + C + D \tag{47c}$$

In the inner region, the mixing length model with  $\chi = 0.41$  gives  $C = 5.28$ . In the outer region, for the flat plate, the solution of (44) gives  $D = 1.76$ .

Table 1 shows the comparison of the reduced friction velocity  $u_\tau/u_e$  obtained from the two methods. Table 1 contains also the Reynolds number  $u_e\theta/\nu$  which is based on the momentum thickness  $\theta$ . Except for low values of the Reynolds number, a good agreement is observed between the two values of the reduced friction velocity which reinforces the validity of the approach used here.

It can be surprising to observe a good agreement between the two methods even when the velocity profiles of Fig. 1 do not exhibit a logarithmic evolution of the velocity whereas law (47c) rests explicitly on the existence of such a logarithmic behaviour. In fact, it is not correct to seek the presence or not of a logarithmic law in Fig. 1. The velocity profiles obtained with SCEM must be compared to a *composite approximation* formed from outer and inner approximations obtained from MMAE [10]. In such a representation, it is possible that the common part—which is precisely the logarithmic law—disappears even if the outer approximation and the inner approximation have a logarithmic part; this happens when the Reynolds number is not large enough.

Table 1

Comparison of  $u_\tau/u_e$  obtained from solution of (45) and from the logarithmic law (47c)

Tableau 1

Comparaison des valeurs de  $u_\tau/u_e$  obtenues d'après la solution de (45) et d'après la loi logarithmique (47c)

$u_\tau \delta/\nu$	$u_e \theta/\nu$	From solution of (45)	Law (47c)
5000	12200	$3.60 \times 10^{-2}$	$3.59 \times 10^{-2}$
1000	2300	$4.20 \times 10^{-2}$	$4.19 \times 10^{-2}$
500	1100	$4.54 \times 10^{-2}$	$4.50 \times 10^{-2}$
250	525	$4.93 \times 10^{-2}$	$4.88 \times 10^{-2}$
100	196	$5.59 \times 10^{-2}$	$5.47 \times 10^{-2}$
50	89	$6.51 \times 10^{-2}$	$6.03 \times 10^{-2}$

6.6. Discussion

The existence of a logarithmic behaviour is very important because the validity of predictions relies on it. It seems that the existence of this law is firmly established [10] but its relation to turbulence models deserves to be discussed.

The arguments used to justify the logarithmic behaviour are based on experimental observations and on the application of MMAE. In the boundary layer, two regions are identified. In the inner region, the length scale is  $\nu/u_\tau$  and the velocity scale is  $u_\tau$ . In the outer region, the length scale is  $\delta$  and the velocity profile is described in terms of a velocity defect  $(u - u_e)/u_\tau$ . The small parameter of the problem is  $u_\tau/u_e$ , the reduced friction velocity, which goes to zero when the Reynolds number  $u_\tau \delta/\nu$  goes to infinity. The first terms of the expansions of the velocity in the inner and outer regions are

$$\frac{u}{u_e} = \frac{u_\tau}{u_e} f\left(\frac{yu_\tau}{\nu}\right) + \dots \tag{48a}$$

$$\frac{u}{u_e} = 1 + \frac{u_\tau}{u_e} g\left(\frac{y}{\delta}\right) + \dots \tag{48b}$$

The validity of these expansions is justified if a matching is possible when  $y^+ \rightarrow \infty$  and  $\eta \rightarrow 0$ . Now, the matching requires that  $f$  and  $g$  have a logarithmic behaviour leading to (47a) and (47b). This solution is valid if  $\chi$  is a finite, non-zero constant. With the overlap hypothesis, the inner and outer domains have a common domain of validity in which the values of  $u$  given by the two logarithmic laws are the same for a given value of  $y$ . Adding member to member (47a) and (47b), we obtain (47c) which gives the evolution of the skin-friction coefficient as a function of the Reynolds number. The skin-friction law (47c) is consistent with the hypothesis  $u_\tau/u_e \rightarrow 0$  as  $u_\tau \delta/\nu \rightarrow \infty$ .

From the above derivation, it seems that the turbulence model does not play any role in the existence of the logarithmic law. However, all the above results have been obtained from experimental results and at the very least, a valuable turbulence model must also include this information. In addition, as stressed by Panton [10], the composite approximation is more important than the inner and outer approximations. Even if the composite approximation exhibits a region of logarithmic behaviour, the above arguments tell us nothing about the extent of this behaviour.

Another argument to derive the logarithmic law is to say that the turbulence time scale is of the order of the inverse of  $\frac{\partial u}{\partial y}$  because the mean shear is at the origin of turbulence and there is a good interaction between turbulence and mean flow. In addition, near the wall, we can assume that the turbulence length scale is the distance to the wall. Then, we have

$$\frac{\partial u}{\partial y} = \frac{u_\tau}{y} \tag{49}$$

where  $u_\tau$  is used as a turbulence velocity scale. The logarithmic law is obtained. This argument is valid if we are not too close to the wall in order to have a fully turbulent regime and if we are not too far away in order to say that the turbulence length scale is the distance to the wall. If we assume that the order of magnitude of the turbulent stress is  $\rho u_\tau^2$ , (49) is an embryo of a turbulence model.

When using SCEM, the necessity of a turbulence model is even clearer since the solution of (41) requires the use of a turbulence model. Then, the validity of the turbulence model can be assessed by comparing results such as those given in Fig. 1 to experimental data. In a way, this point of view is more satisfactory than saying that a turbulence

model is not required to derive the logarithmic law. In addition, the use of a turbulence model gives obviously much more precise information on the behaviour of the solution. For example, we can determine the extension of the logarithmic behaviour of the composite approximation and the value of the Reynolds number below which this behaviour disappears.

## 7. Conclusion

The idea of interactive boundary layer (IBL) is not new since this notion has been extensively applied to calculate flows around airfoils or wings [3–6]. Rational arguments to support this approach were missing until now [21]. Here, in turbulent flow, this lack is filled with a full justification thanks to the application of the successive complementary expansion method (SCEM) in its generalized form.

Uniformly valid approximations (UVAs) obtained with the method of matched asymptotic expansions (MMAE) and SCEM are different because MMAE is based on *regular expansions*. A major consequence is that the wall boundary condition for the first order inviscid flow approximation in MMAE is a zero normal velocity. It results that a *hierarchy* is established between the inviscid and viscous sets of equations which can be solved *sequentially*. At first, the inviscid flow equations are solved *independently* from the boundary layer equations. In the second step, the boundary layer equations are solved using results obtained from the previous calculation. In the third step, the solution of the second order inviscid flow equations takes into account the boundary layer effects and provides a correction to the first estimate. Finally, the second order boundary layer can be calculated. With IBL, the hierarchy between the inviscid flow equations and the boundary layer is broken. The condition of zero normal velocity at the wall for the inviscid flow is replaced by the condition that the difference between the viscous and inviscid normal velocities tends towards zero far away from the wall. Consequently, *the inviscid flow equations and the boundary layer equations interact*. One system of equations influences the other and vice versa. The two sets of equations must be solved simultaneously. With appropriate numerical techniques, IBL model lets us calculate separated flows.

In the study of the turbulent boundary layer with MMAE, a striking feature is the logarithmic overlap region between the inner and outer regions. The existence of this behaviour is obtained without using a turbulence model but, obviously, the experimental knowledge is essential to set the starting hypotheses. Now, to calculate a boundary layer, it is necessary to implement such a model. The conclusion is that the turbulence model must be compatible with the existence of a logarithmic evolution of the velocity.

With SCEM, the issue is addressed differently because there is no overlap condition. Therefore, the result depends on the turbulence model. For the case of the flat plate flow, the numerical results show that the model used here, a simple mixing length model, leads us to results which have, at least, a correct qualitative behaviour. This model has been used for the purpose of demonstration. For more accurate applications, more sophisticated models are required and the assessment of their validity implies comparisons with experimental data.

## References

- [1] S.B. Pope, Turbulent Flows, Cambridge University Press, Cambridge, UK, 2000.
- [2] P.A. Bois, Joseph Boussinesq, a pioneer of Mechanical Modelling at the end of the 19th century, C. R. Mecanique 335 (2007), this issue, DOI:10.1016/j.crme.2007.08.002.
- [3] J.E. Carter, A new boundary layer inviscid iteration technique for separated flow, AIAA Paper 79-1450, in: 4th Computational Fluid Dynamics Conf., Williamsburg, 1979.
- [4] T. Cebeci, An Engineering Approach to the Calculation of Aerodynamic Flows, Horizons Publishing Inc., Springer-Verlag, Long Beach, CA, Berlin, 1999.
- [5] J.C. Le Balleur, Couplage visqueux–non visqueux : analyse du problème incluant décollements et ondes de choc, La Recherche Aérospatiale 6 (1977) 349–358.
- [6] A.E.P. Veldman, Matched asymptotic expansions and the numerical treatment of viscous–inviscid interaction, J. Eng. Math. 39 (2001) 189–206.
- [7] J. Cousteix, J. Mauss, Analyse asymptotique et couche limite, Mathématiques et Applications, vol. 56, Springer-Verlag, SMAI, Berlin, Heidelberg, 2006.
- [8] J.J. Mahony, An expansion method for singular perturbation problems, J. Austral. Math. Soc. 2 (1962) 440–463.
- [9] R.E. O'Malley Jr., Introduction to Singular Perturbations, Applied Mathematics and Mechanics, vol. 14, Academic Press, New York, London, 1974.
- [10] R.L. Panton, Review of wall turbulence as described by composite expansions, Appl. Mech. Rev. 58 (1) (January 2005) 1–36.
- [11] W.W. George, Recent advancements toward the understanding of turbulent boundary layers, AIAA J. 44 (2006) 2435–2449.

- [12] G.L. Mellor, The large Reynolds number asymptotic theory of turbulent boundary layers, *Int. J. Eng. Sci.* 10 (1972) 851–873.
- [13] K.S. Yajnik, Asymptotic theory of turbulent shear flows, part 2, *J. Fluid Mech.* 42 (1970) 411–427.
- [14] R. Michel, C. Quémard, R. Durant, Application d'un schéma de longueur de mélange à l'étude des couches limites turbulentes d'équilibre, N.T. 154, ONERA, 1969.
- [15] E.R. Van Driest, On turbulent flow near a wall, *J. Aeron. Sci.* 23 (1956) 1007.
- [16] F.H. Clauser, The turbulent boundary layer, *Adv. Appl. Mech.* 4 (1956) 1–51.
- [17] D. Coles, The law of the wake in the turbulent boundary layer, *J. Fluid Mech.* 1 (1956) 191.
- [18] D. Coles, Remarks on the equilibrium turbulent boundary layer, *J. Aero. Sci.* 24 (1957).
- [19] G.L. Mellor, D.M. Gibson, Equilibrium turbulent boundary layer, FLD No. 13, Princeton University, 1963.
- [20] J.C. Rotta, Turbulent Boundary Layers in Incompressible Flows, *Progress in Aeronautical Sciences*, vol. 2, Pergamon Press, 1962.
- [21] V.V. Sychev, A.I. Ruban, Vic.V. Sychev, G.L. Korolev, Asymptotic Theory of Separated Flows, Cambridge University Press, Cambridge, UK, 1998.